Biomedicine & Pharmacotherapy 177 (2024) 117059

Contents lists available at ScienceDirect

Biomedicine & Pharmacotherapy

journal homepage: www.elsevier.com/locate/biopha

Ruthenium complex containing 1,3-thiazolidine-2-thione inhibits hepatic cancer stem cells by suppressing Akt/mTOR signalling and leading to apoptotic and autophagic cell death

Sara P. Neves [a], Larissa M. Bomfim [a], Tetsushi Kataura [b], Sabrine G. Carvalho [a], Mateus L. Nogueira [a], Rosane B. Dias [a,c,d], Ludmila de F. Valverde [a,e], Clarissa A. Gurgel Rocha [a,c,f], Milena B.P. Soares [a,g], Monize M. da Silva [h], Alzir A. Batista [h], Viktor I. Korolchuk [b], Daniel P. Bezerra [a,*]

[a] Gonçalo Moniz Institute, Oswaldo Cruz Foundation (IGM-FIOCRUZ/BA), Salvador, Bahia, 40296-710, Brazil
[b] Biosciences Institute, Faculty of Medical Sciences, Newcastle University, Newcastle upon Tyne, NE4 5PL, UK
[c] Department of Propedeutics, School of Dentistry of the Federal University of Bahia, Salvador, Bahia, 40110-909, Brazil
[d] Department of Biological Sciences, State University of Feira de Santana, Feira de Santana, Bahia, 44036-900, Brazil
[e] Department of Dentistry, Federal University of Sergipe, Lagarto, Sergipe, 49400-000, Brazil
[f] Center for Biotechnology and Cell Therapy, D'Or Institute for Research and Education (IDOR), Salvador, Bahia, 41253-190, Brazil
[g] SENAI Institute of Innovation (ISI) in Health Advanced Systems, University Center SENAI/CIMATEC, Salvador, Bahia, 41650-010, Brazil
[h] Department of Chemistry, Federal University of São Carlos, São Carlos, São Paulo, 13561-901 Brazil

ARTICLE INFO

Keywords:
Ruthenium complex
Hepatic cancer stem cells
HCC
Apoptosis
Autophagy
Mitophagy

ABSTRACT

Hepatic cancer is one of the main causes of cancer-related death worldwide. Cancer stem cells (CSCs) are a unique subset of cancer cells that promote tumour growth, maintenance, and therapeutic resistance, leading to recurrence. In the present work, the ability of a ruthenium complex containing 1,3-thiazolidine-2-thione (RCT), with the chemical formula $[Ru(tzdt)(bipy)(dppb)]PF_6$, to inhibit hepatic CSCs was explored in human hepatocellular carcinoma HepG2 cells. RCT exhibited potent cytotoxicity to solid and haematological cancer cell lines and reduced the clonogenic potential, $CD133^+$ and $CD44^{high}$ cell percentages and tumour spheroid growth of HepG2 cells. RCT also inhibited cell motility, as observed in the wound healing assay and transwell cell migration assay. RCT reduced the levels of Akt1, phospho-Akt (Ser473), phospho-Akt (Thr308), phospho-mTOR (Ser2448), and phospho-S6 (Ser235/Ser236) in HepG2 cells, indicating that interfering with Akt/mTOR signalling is a mechanism of action of RCT. The levels of active caspase-3 and cleaved PARP (Asp214) were increased in RCT-treated HepG2 cells, indicating the induction of apoptotic cell death. In addition, RCT modulated the autophagy markers LC3B and p62/SQSTM1 in HepG2 cells and increased mitophagy in a mt-Keima-transfected mouse embryonic fibroblast (MEF) cell model, and RCT-induced cytotoxicity was partially prevented by autophagy inhibitors. Furthermore, mutant $Atg5^{-/-}$ MEFs and PentaKO HeLa cells (human cervical adenocarcinoma with five autophagy receptor knockouts) were less sensitive to RCT cytotoxicity than their parental cell lines, indicating that RCT induces autophagy-mediated cell death. Taken together, these data indicate that RCT is a novel potential anti-liver cancer drug with a suppressive effect on CSCs.

1. Introduction

Hepatic cancer is one of the leading causes of cancer-related death worldwide, with approximately 905,700 new cases and 830,200 deaths worldwide in 2020. By 2040, 1.3 million people are expected to die from liver cancer [1].

Hepatocellular carcinoma (HCC) is the most frequent histologic type of liver cancer, accounting for 90 % of all liver cancer cases. Systemic therapies are recommended for patients with advanced or intermediate HCC, and sorafenib and lenvatinib continue to be the most effective single-drug treatments [2–5]. As second-line therapies, regorafenib, cabozantinib, and ramucirumab have shown enhanced survival

* Corresponding author.
E-mail address: daniel.bezerra@fiocruz.br (D.P. Bezerra).

https://doi.org/10.1016/j.biopha.2024.117059

Available online 1 July 2024

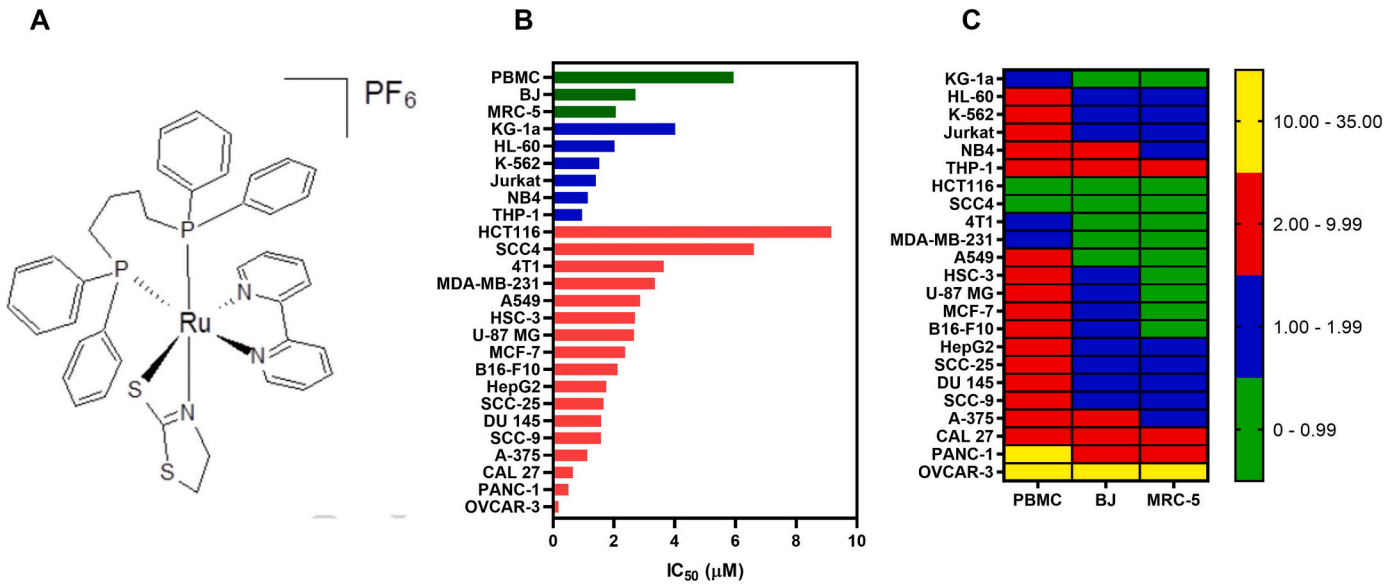

Fig. 1. (A) Chemical structure of RCT. (B) IC_{50} values for the cytotoxicity of RCT against solid (red bars) and haematological cancers (blue bars), as well as against noncancerous cells (green bars). (C) Heatmap of selectivity indices (SIs) obtained for RCT. The SI was calculated using the following formula: SI = IC_{50} [noncancerous cells]/IC_{50} [cancer cells].

advantages [6–8]. However, new drugs are urgently needed to improve HCC treatment and patient survival.

Cancer stem cells (CSCs) are a unique subset of cancer cells that promote tumour formation, maintenance, and resistance to therapy, eventually leading to recurrence. These cells have stem cell features and dictate a hierarchical organization [9–11]. Dysregulation of cell metabolism and cell signalling pathways has been described in the pathogenesis of CSCs and has been reported to be a target for eradicating this rare population of cancer cells [9,10,12,13].

Ruthenium complexes have been reported as a potential new class of antineoplastic agent with effects on different types of cancer cells [14–19]. A ruthenium complex containing 1,3-thiazolidine-2-thione (RCT) (Fig. 1A), with the chemical formula [Ru(tzdt)(bipy)(dppb)]PF_6 (where tzdt = 1,3-thiazolidine-2-thione, bipy = 2,2′-bipyridine and dppb = 1,4-bis(diphenylphosphino)butane), was previously synthesized by our group and exhibited potent cytotoxicity against cancer cells with the ability to inhibit the topoisomerase IB enzyme [20,21]. In HCC HepG2 cells, RCT suppressed cell growth in two-dimensional and three-dimensional models, caused caspase-mediated cell death via ERK1/2 signalling through ROS- and p53-independent pathways, and reduced tumour growth in vivo in a HepG2 xenograft model with tolerable toxicity [22].

In the present work, the ability of RCT to inhibit hepatic CSCs was explored in HCC HepG2 cells. We found that RCT suppresses hepatic CSCs by inhibiting Akt/mTOR signalling and causing apoptotic and autophagic cell death.

2. Materials and methods

2.1. RCT synthesis

RCT was synthesized and characterized as previously described [20,21]. For all experiments, RCT was dissolved in sterile dimethyl sulfoxide (DMSO, Synth, Diadema, SP, Brazil) in a 5 mg/mL stock solution and diluted with culture medium to various concentrations.

2.2. Cell culture

A panel of 23 cancer cell lines, two noncancerous cell lines, one primary noncancerous cell line and three mutant cell lines, as well as their parental cell lines, were used in this study (as specified in Supplementary Table 1). The cells were cultivated according to the manufacturer's instructions for each cell line or the ATCC recommendations for animal cell culture [23]. All cell lines were grown in flasks at 37 °C with 5 % CO_2 and subcultured every 3–4 days to sustain exponential growth. Adherent cells were collected using a 0.25 % trypsin-EDTA solution (Sigma Aldrich Co.). To confirm the use of mycoplasma-free cells, all cell lines were screened for mycoplasma using a mycoplasma staining kit (Sigma Aldrich).

2.3. Alamar blue assay

Cell viability was quantified using the Alamar blue assay, as previously described [24]. Adherent cells were plated in 96-well plates at a density of 7×10^3 cells/well, and 3×10^4 cells/well were used for suspension. Drugs were added to each well after overnight incubation for adherent cells or immediately after seeding for suspension cells, and incubation continued for an additional 72 h. Doxorubicin was used as a positive control (Laboratorio IMA S.A.I.C., Buenos Aires, Argentina). Four hours (for cell lines) or 24 h (for primary cultures) before the end of incubation, 20 μL of resazurin (30 μM) (Sigma—Aldrich Co. St. Louis, MO, USA) was added to each well. The absorbance at 570 and 600 nm was quantified using a SpectraMax 190 microplate reader (Molecular Devices, Sunnyvale, CA, USA).

2.4. Colony-forming assay

To assess clonogenic potential, 500 cells were plated in 6-well plates with 6 mL of complete medium and treated with drugs for 24, 48, or 72 h. Then, the medium was replaced with fresh medium without drugs, and the cells were cultivated for a total of 14 days. Next, the cells were fixed in methanol and stained with 0.5 % crystal violet. The number of colonies containing more than 50 cells was counted using an optical microscope (Nikon, TS100).

2.5. HepG2 tumour spheroids

HepG2 cells were plated in 24-well low-adhesion plates (Corning, USA) at a low cell density (1000 cells/well in 2 mL) with serum-free DMEM-F12 supplemented with 20 ng/mL bFGF (PeproTech, USA),

20 ng/mL EGF (PeproTech, USA), and B27 supplement (Invitrogen, Carlsbad, CA, USA). After five days of incubation, the cells were treated with RCT at 20, 10, 5, 2.5, or 1.25 μM. A Leica DMI8 optical microscope was used to image the cells after 0, 24, and 48 h of incubation. For confocal microscopy, cells were treated with 5 μM RCT for 48 h, stained with acridine orange (1 μg/mL) plus propidium iodide (PI, 1 μg/mL), and examined using a Leica TCS SP8 confocal microscope (Leica Microsystems, Wetzlar, HE).

2.6. Flow cytometry assay

Flow cytometry was used to quantify protein levels using primary antibodies conjugated to fluorochromes, as described in Supplementary Table 2. For cell surface protein staining, the cells were rinsed with an incubation buffer (0.5 % bovine serum albumin in PBS), and then antibodies were added and incubated for 1 h at room temperature. After the cells were washed with PBS, the fluorescence of the cells was evaluated using flow cytometry. To select live cells for the quantification of CD133-positive cells, YO-PRO-1 (Sigma Aldrich Co.) was used.

For intracellular protein staining, the cells were collected and resuspended in 0.5–1 mL of 4 % formaldehyde for 10 min at 37 °C. The tube was then placed on ice for 1 min. The cells were permeabilized on ice for 30 min by progressively adding ice-cold 100 % methanol to prechilled cells with gentle vortexing until the final methanol concentration reached 90 %. After washing with incubation buffer (0.5 % bovine serum albumin in PBS), antibodies were added, and the cells were incubated at room temperature for 1 h. Finally, the cells were rinsed with PBS, and cell fluorescence was evaluated by flow cytometry.

Internucleosomal DNA fragmentation and cell cycle distribution were examined by DNA content. The cells were stained with PI using a solution containing 0.1 % Triton X-100, 2 μg/mL PI, 0.1 % sodium citrate, and 100 μg/mL RNAse (all from Sigma—Aldrich) and incubated in the dark for 15 min at room temperature [25]. Cellular fluorescence was quantified by flow cytometry.

Cell viability was also examined by an Annexin V-FITC/PI (FITC Annexin V Apoptosis Detection Kit I, BD Biosciences, San Jose, CA, USA) according to the manufacturer's instructions. Cellular fluorescence was quantified by flow cytometry.

For the functional assay, the following inhibitors were used: chloroquine (autophagy inhibitor, Sigma—Aldrich Co.); 3-methyladenine (3-MA, autophagy inhibitor, Sigma—Aldrich Co.); or bafilomycin A1 (autophagy inhibitor, Enzo Life Sciences).

For all flow cytometry analyses, cellular fluorescence was quantified using a BD LSRFortessa cytometer (BD Biosciences), BD FACSDiva software (BD Biosciences), and FlowJo software 10 (FlowJo LLC; Ashland, OR, USA). A minimum of 10^4 events/sample were analysed for intracellular staining, and a minimum of 3×10^4 events/sample were analysed for cell surface protein staining. Cellular debris was excluded, and single cells were selected using FSC-A *vs* FCS-H and SCC-A *vs* SCC-H.

2.7. Wound healing assay

Wound healing assays were performed as previously described [26], with minimal modifications. The cells were grown to 80–90 % confluency in 12-well plates, and a wound was produced by dragging a plastic pipette tip over the cell surface. The remaining cells were washed three times with saline solution to remove cell debris before they were grown in serum-free medium and treated with drugs. Migrating cells in front of the wound were imaged using an optical microscope (Nikon TS 100) after 0, 24, 48 and 72 h of incubation. The wound area was determined using ImageJ software from the National Institutes of Health (NIH, USA).

2.8. Transwell migration assay

Transwell plates were also used for the cell migration assay, which was performed as previously described [27]. The cells were first treated in serum-free medium for 24 h. In 6-well plates (8 μm pore size; Corning, USA), we used uncoated cell culture inserts. The upper chamber received 1.5 mL of serum-free medium, whereas the lower chamber received 2 mL of 20 % FBS medium. Cells that remained in the top compartment after 24 h were removed with cotton swabs. The cells on the bottom surface of the membrane were fixed with 4 % paraformaldehyde and stained with 0.5 % crystal violet. An optical microscope (Leica DMI8) was used to image and count the cells.

2.9. qPCR array

Total RNA was extracted using the RNeasy plus Mini Kit (Qiagen; Hilden, Germany) according to the manufacturer's instructions. A NanoDrop® 1000 spectrophotometer (Thermo Fisher Scientific, Waltham, Massachusetts, USA) was used to analyse and quantify the purity of the RNA. A Superscript VILO™ Kit (Invitrogen Corporation, Waltham, MA, USA) was used for RNA reverse transcription. A TaqMan® array human cancer drug target 96-well plate, fast (ID RPRWENH, Applied Biosystems™, Foster City, CA, USA) was utilized for gene expression measurement through qPCR. The analyses were carried out using ABI ViiA7 (Applied Biosystems™) equipment.

The cycle conditions were 2 min at 50 °C, 10 min at 95 °C, and 40 cycles of 15 s at 95 °C and 1 min at 60 °C. All the experiments were conducted under DNase/RNase-free conditions. The $2^{-\Delta\Delta CT}$ method [28] was applied to calculate the relative quantification (RQ) of mRNA expression using Gene Expression Suite™ Software (Applied Biosystems™). Cells treated with the negative control (0.2 % DMSO) were used as a calibrator, and the RQs of the reference genes *GAPDH*, *B2M* and *RPLP0* were used to normalize the responses. When RQ was ≤ 0.5, the genes were considered downregulated, indicating that gene expression in drug-treated cells was at least half that of negative control-treated cells, while when RQ was ≥ 2, the genes were deemed upregulated, indicating that gene expression in drug-treated cells was at least double that in negative control-treated cells.

2.10. Immunofluorescence staining

The cells were cultivated on coverslips in 24-well plates for 24 h before being treated with drugs. After that, the cells were rinsed twice with saline solution, permeabilized with 0.5 % Triton X-100, treated with RNAse (10 μg/mL), and incubated overnight with a fluorochrome-conjugated primary antibody (detailed in Supplementary Table 2). The cells were rinsed with saline solution the next day and mounted using Fluoromount-G with DAPI (Invitrogen, Thermo Fisher Scientific). A Leica TCS SP8 confocal microscope (Leica Microsystems, Wetzlar, HE, Germany) was used to photograph the cells.

2.11. Transmission electron microscopy analysis

The cells were fixed in 0.1 M sodium cacodylate buffer (pH 7.4) containing 2.5 % glutaraldehyde and 2 % paraformaldehyde for at least 2 h. Following rinsing, the cells were exposed to 1 % osmium tetroxide, 0.8 % potassium ferricyanide, and 5 mM calcium chloride for 1 h. The cells were then washed again and dehydrated in an acetone series before being embedded in polybed epoxy resin. The ultrathin slices were stained with 2 % aqueous uranyl acetate and 2 % aqueous lead citrate and analysed by transmission electron microscopy (TEM) using a JEM-1230 microscope (JEOL, 1230, USA, Inc.).

2.12. Mitophagy assay

Wild-type MEFs stably expressing mt-Keima were cultured in small plates for 24 h (Greiner Bio-One). After this period, the cells were treated with 4 μM RCT or with 1.5 mL of acetoacetate [29] or galactose [30] media. The mt-Keima live cell signal was acquired using a Leica

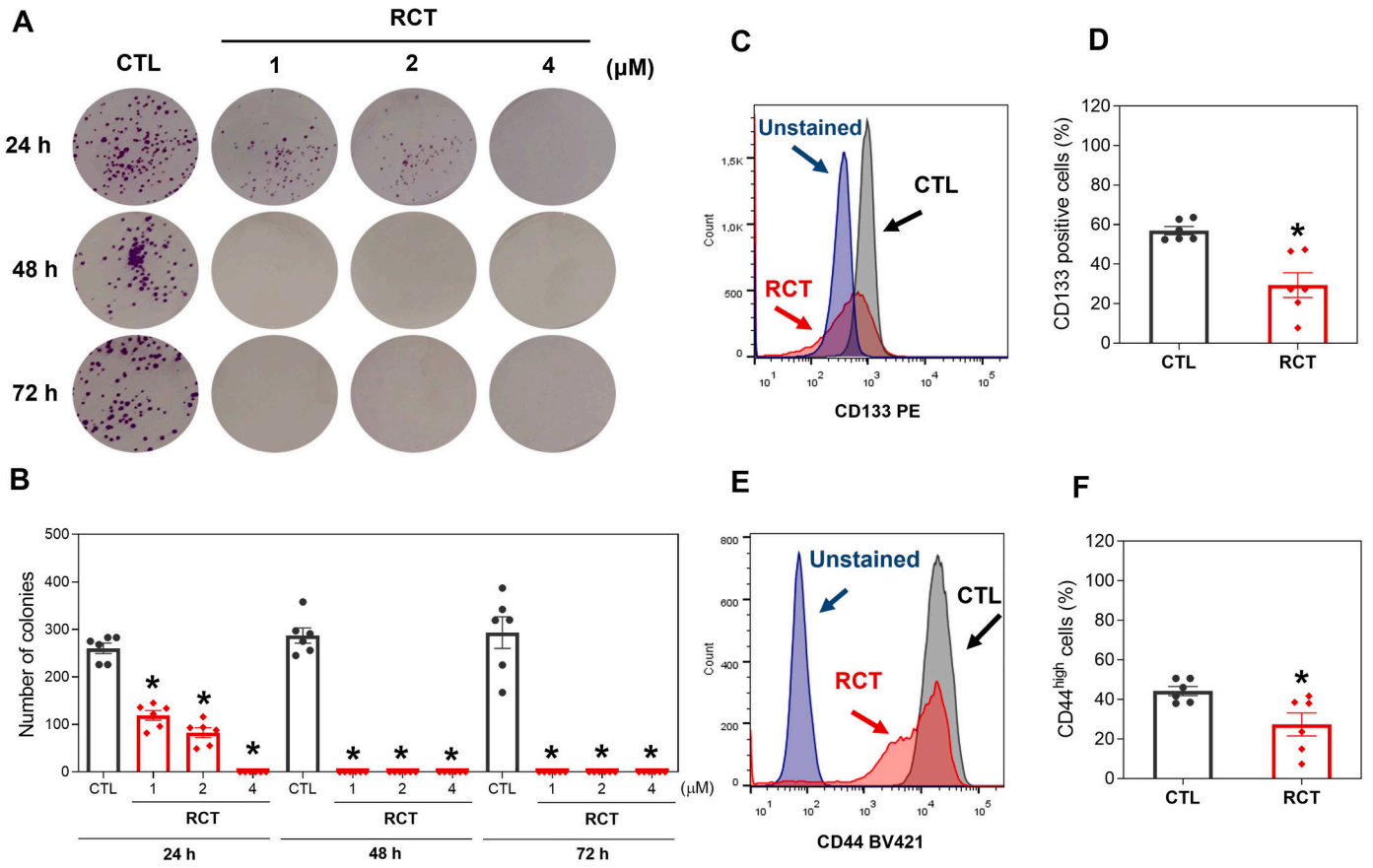

Fig. 2. (A) Representative images and (B) quantification of the number of colonies formed from HepG2 cells after treatment with RCT. (C and D) Quantification of CD133 expression on HepG2 cells after 24 h of incubation with 4 μM RCT, as determined by flow cytometric analysis. (E and F) Quantification of $CD44^{high}$ in HepG2 cells after 24 h of incubation with 4 μM RCT, as determined by flow cytometric analysis. The vehicle (0.2 % DMSO) was used as a control (CTL). The data are reported as the mean ± S.E.M. from three independent experiments, each performed in duplicate. * $P < 0.05$ compared to CTL by one-way ANOVA followed by Dunnett's multiple comparisons test or Student's *t* test.

DMi8 inverted microscope with a Plan-Apochromat 63x/1.30 oil immersion objective equipped with an ORCA-Flash4v2.0 camera (Hamamatsu). Mitophagy events were determined as the number of points per cell in images generated by subtracting the signal at 480 nm excitation (indicating a neutral pH environment) from the signal at 561 nm excitation (indicating an acidic pH environment) by using ImageJ (version 1.41; NIH).

2.13. Statistical analysis

The data are reported as the mean ± S.E.M. or displayed as cell popular violin plots or as half-maximal inhibitory concentration (IC_{50}) values with a 95 % confidence interval from at least three independent experiments (biological replicates), each performed in duplicate (technical replicates). The selectivity indices were calculated using the following formula: selectively indices = IC_{50} [noncancerous cells]/IC_{50} [cancer cells]. Using GraphPad Prism (Intuitive Software for Science; San Diego, CA, USA), two-tailed unpaired Student's *t* test ($P < 0.05$) was used to compare data between two groups, and one-way analysis of variance (ANOVA) followed by Dunnett's multiple comparisons test ($P < 0.05$) was used to compare data among three or more groups.

3. Results

3.1. RCT exhibits potent cytotoxicity to solid and haematological cancer cells

The cytotoxic potential of RCT was evaluated in 23 cancer cell lines of different histological types after 72 h of incubation by the alamar blue method. The RCT showed potent cytotoxicity for different cell types, including solid (HepG2, HCT116, MDA-MB-231, MCF-7, 4T1, HSC-3, CAL 27, SCC-25, SCC-4, SCC-9, A549, PANC-1, OVCAR-3, DU 145, U-87 MG, A-375, and B16-F10) and haematological (NB4, THP-1, Jurkat, K-562, HL-60, and KG-1a) malignancies (Fig. 1B and Supplementary Table 3). For solid cancer cell lines, RCT showed IC_{50} values ranging from 0.18 μM for ovarian cancer OVCAR-3 cells to 9.16 μM for colon carcinoma HCT116 cells. For haematological malignancies, RCT showed IC_{50} values ranging from 0.95 μM for monocytic leukaemia THP-1 cells to 4.02 μM for acute myeloid leukaemia KG-1a cells. Doxorubicin, used as a positive control, exhibited IC_{50} values ranging from 0.03 μM for melanoma A-375 cells to 4.43 μM for oral squamous cell carcinoma SCC-4 cells.

For comparison with that of malignant cells, the cytotoxic potential of RCT was also investigated in three noncancerous cell lines (PBMC, MRC-5, and BJ). In noncancerous cells, RCT had IC_{50} values of 5.94 μM for PBMCs, 2.71 μM for foreskin fibroblast BJ cells and 2.06 μM for lung fibroblast MRC-5 cells. The selectivity indices (SIs) were calculated for each cell line and are displayed in Fig. 1**C** and Supplementary Table 4. Importantly, RCT showed an SI greater than 2 for many of the cells tested, especially compared with PBMCs. The IC_{50} values of doxorubicin were 1.44 μM for PBMCs, 1.85 μM for foreskin fibroblast BJ cells and 0.39 μM for lung fibroblast MRC-5 cells.

In addition to being among the lines with good selectivity indices, HCC HepG2 cell line was among the most sensitive cancer cell lines to RCT and was selected for this study to evaluate the potential of RCT against liver CSCs.

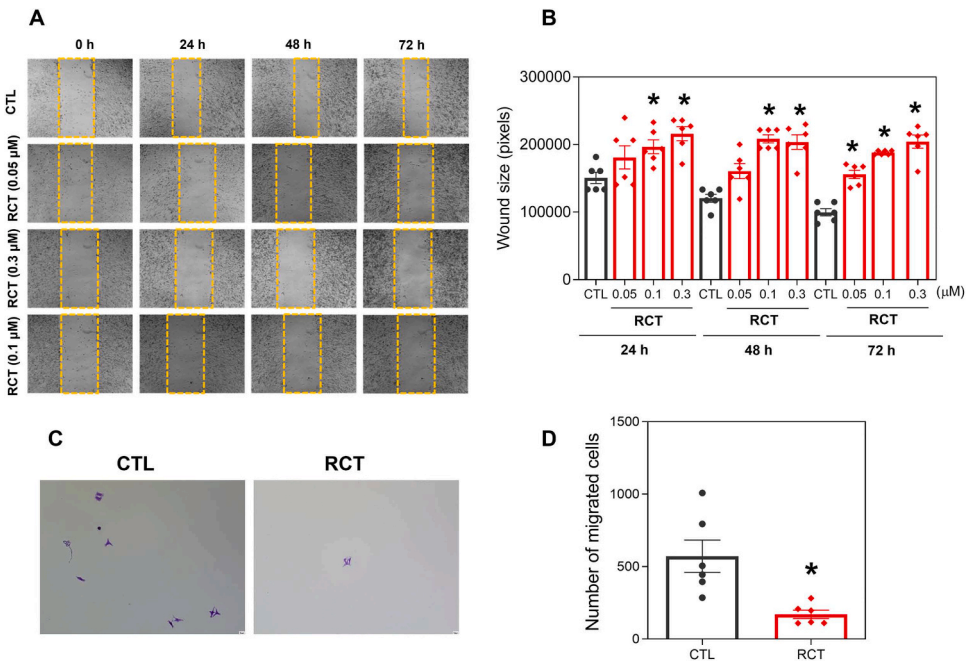

Fig. 3. (A) Representative images and (B) quantification of HepG2 cell migration in the wound healing assay after 24, 48 and 72 h of incubation with RCT. (C) Representative images and (D) quantification of HepG2 cell migration in the transwell migration assay after 24 h of incubation with 4 μM RCT. The vehicle (0.2 % DMSO) was used as a control (CTL). The data are reported as the mean ± S.E.M. from three independent experiments, each performed in duplicate. * $P < 0.05$ compared to CTL by one-way ANOVA followed by Dunnett's multiple comparisons test or Student's *t* test.

3.2. RCT causes elimination of hepatic CSCs from HCC HepG2 cells

To evaluate the potential of RCT for the treatment of hepatic CSCs, we first analysed the effect of RCT on the clonogenic potential of HepG2 cells. The clonogenic assay, also known as the colony formation assay, is a well-established in vitro approach for assessing CSC survival and proliferation [31]. Furthermore, the hepatic cell surface CSC markers CD133 and CD44 [32] were analysed in RCT-treated HepG2 cells. Finally, we evaluated the effect of RCT on HepG2 tumour spheroids as a method to enrich cell culture with CSCs [33].

The clonogenic potential of HepG2 cells was determined after treatment with RCT at concentrations of 1, 2, and 4 μM for 24, 48, and 72 h of incubation. Treatment of HepG2 cells with RCT reduced colony formation in a time- and concentration-dependent manner (Fig. 2A and B). The inhibition rates were 54.7, 68.6 and 100 % after 24 h of incubation, respectively, and 100 % for all concentrations tested after 48 and 72 h of incubation.

RCT reduced the number of HepG2 CD133-positive cells after 24 h of incubation. At a concentration of 4 μM, RCT reduced the percentage of HepG2 CD133-positive cells to 29.9 % compared with 57.8 % detected in the control (Fig. 2C and D). A reduction in $CD44^{high}$ cells was also detected after treatment with RCT at the same concentration for 24 h (Figs. 2E and F).

In the HepG2 tumour spheroid model, RCT reduced tumour spheroid growth (Supplementary Figure 1) and caused cell death (Supplementary Figure 2), indicating the anti-CSC potential of RCT.

3.3. RCT inhibits HCC HepG2 cell motility

Considering that RCT reduces hepatic CSCs and that one of the characteristics of CSCs is their strong migratory and metastatic potential [34], we hypothesized that RCT could have antimigration potential. Therefore, the motility of the RCT-treated HepG2 cells was assessed by a wound healing assay (Fig. 3A and B) and a transwell cell migration assay (Fig. 3C and D). First, noncytotoxic concentrations of RCT were screened (Supplementary Figure 3) for use in the wound healing assay. Next, we found that RCT reduces HepG2 cell migration potential in both models.

3.4. RCT suppresses Akt/mTOR signalling in HCC HepG2 cells

The molecular mechanism of action of RCT in HepG2 cells was investigated by analysing the transcripts of 82 target genes using a qPCR array (Fig. 4A and Supplementary Table 5). A total of 21 genes were upregulated, and 6 genes were downregulated, including *PRKCB* (RQ = 0.333), in RCT-treated HepG2 cells. This gene encodes the protein kinase C beta enzyme, which interacts with protein kinase B, better known as Akt [35]. Therefore, the protein levels of several elements of the Akt/mTOR signalling pathway were measured.

Curiously, the expression levels of Akt1 (Fig. 4B and C) and the levels of phosphorylated Akt at Ser 473 (Fig. 4D and E), Akt at Thr 308 (Fig. 4F and G), mTOR at Ser 2448 (Fig. 4H and I), and S6 at Ser 235/Ser 236 (Fig. 4J and K) were reduced in HepG2 cells treated with RCT, indicating that interference with Akt/mTOR signalling is the mechanism of action of RCT. The levels of phosphorylated PI3K p85/p55 at Tyr 458/Tyr 199 (Supplementary Figure 4A and B), 4EBP1 at Thr 36/Thr 45 (Supplementary Figure 4C and D) and elF4E at Ser 209 (Supplementary Figure 4E and F) were not altered.

NF-κB signalling involves crosstalk with Akt/mTOR signalling [36] and has also been investigated. However, the levels of NF-κB p65 phosphorylated at Ser 529 (Supplementary Figure 5A and B) and NF-κB p65 phosphorylated at Ser 536 (Supplementary Figure 5C and D) and the level of IκBα (Supplementary Figure 5E and F) were not changed in the RCT-treated HepG2 cells.

3.5. RCT induces apoptotic and autophagic cell death in HCC HepG2 cells

The type of cell death induced by RCT in HepG2 cells was also investigated. First, the levels of active caspase-3 (Fig. 5A and B) and cleaved PARP (Asp214) (Fig. 5C and D) were measured in RCT-treated HepG2 cells to investigate apoptotic cell death. Interestingly, at a concentration of 4 μM, RCT increased the levels of these two apoptotic cell death markers after 24 h of incubation, indicating the induction of

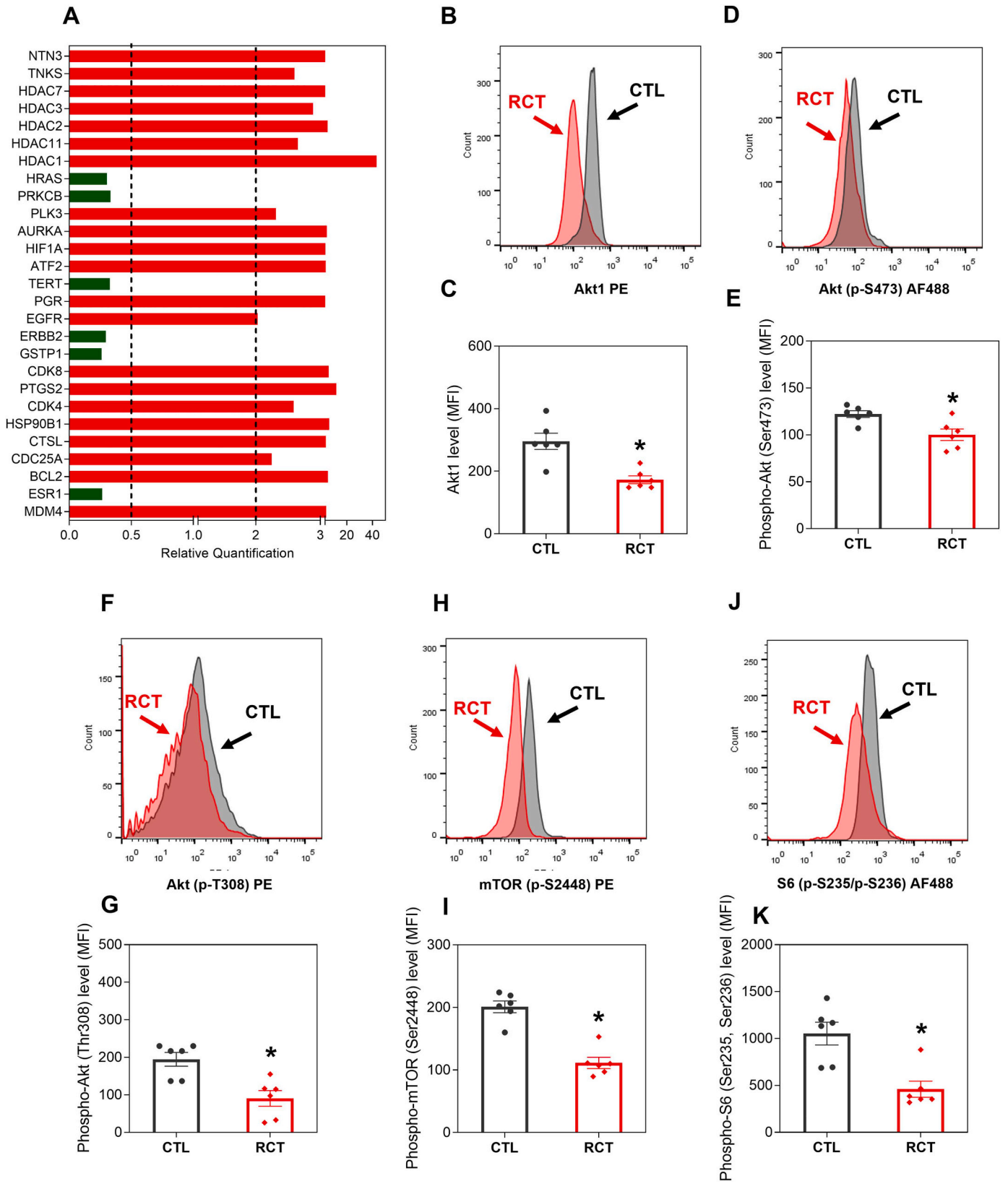

Fig. 4. (A) Genes up- and downregulated in HepG2 cells after 12 h of treatment with 4 μM RCT. The vehicle (0.2 % DMSO) was used as a control (CTL). The data are shown as relative quantification compared to CTL. The genes were upregulated if RQ ≥ 2 (red bars) and downregulated if RQ ≤ 0.5 (green bars). Quantification of the levels of Akt1 (B and C), phospho-Akt (Ser473) (D and E), phospho-Akt (Thr308) (F and G), phospho-mTOR (Ser2448) (H and I) and phospho-S6 (Ser235/Ser236) (J and K) in HepG2 cells after 24 h of incubation with 4 μM RCT, as determined by flow cytometric analysis. The vehicle (0.2 % DMSO) was used as a control (CTL). The data are reported as the mean ± S.E.M. from three independent experiments, each performed in duplicate. * $P < 0.05$ compared to CTL by Student's *t* test. MFI: Mean fluorescence intensity.

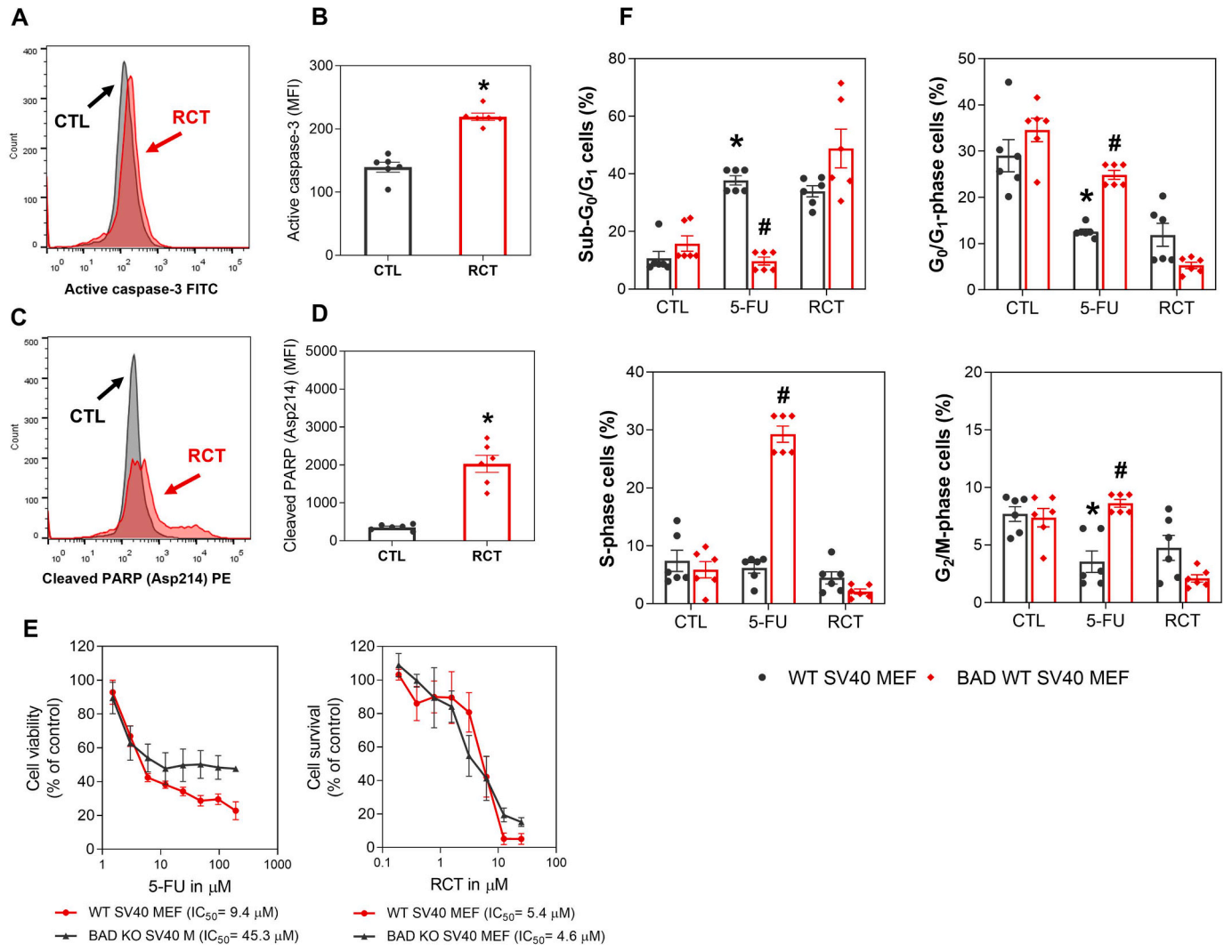

Fig. 5. Quantification of the levels of active caspase-3 (A and B) and cleaved PARP (Asp214) (C and D) in HepG2 cells after 24 h of incubation with 4 μM RCT, as determined by flow cytometric analysis. (E) Survival curves of WT SV40 MEFs and BAD KO SV40 MEFs upon treatment with 5-fluorouracil (5-FU, used as a positive control) and RCT. The curves were obtained from at least three independent experiments performed in duplicate using the Alamar blue assay after 72 h of incubation. (F) Cell cycle distribution of WT SV40 MEFs and BAD KO SV40 MEFs after 48 h of incubation with 40 μM 5-FU or 2 μM RCT. The vehicle (0.2 % DMSO) was used as a control (CTL). The data are reported as the mean ± S.E.M. from three independent experiments, each performed in duplicate. * $P < 0.05$ compared to CTL by one-way ANOVA followed by Dunnett's multiple comparisons test or Student's *t* test. MFI: Mean fluorescence intensity.

apoptotic cell death by RCT in HepG2 cells.

Since mouse embryonic fibroblasts (MEFs) are good models for studying gene knockout functions [37,38], the role of the proapoptotic protein BAD in RCT-induced cell death was also investigated using immortalized MEFs generated from *Bad* gene-knockout (BAD-KO SV40 MEFs) and the parental cell line wild-type (WT SV40 MEFs). However, RCT was able to induce cell death independent of the BAD protein (Fig. 5E and F).

Next, we evaluated whether RCT could modulate autophagy. The protein expression levels of the autophagy markers LC3B and p62/SQSTM1 were quantified in RCT-treated HepG2 cells. After 24 h of incubation, RCT treatment increased the level of LC3B (Fig. 6A), as observed by flow cytometry analyses, and decreased the level of p62/SQSTM1 (Fig. 6B and C), as detected by flow cytometry and confocal microscopy analysis, indicating the induction of autophagy by RCT in HepG2 cells. In addition, autophagic vacuoles were found in RCT-treated HepG2 cells by MET analysis (Fig. 6D).

As mt-Keima-expressing MEFs are useful models for monitoring mitophagy [39], a type of autophagy-mediated selective mitochondrial degradation, wild-type MEFs transfected with mt-Keima were used to investigate whether RCT could induce mitophagy. Compared with the negative control, 2 μM RCT increased mitophagy events after 24 (Fig. 7A and B) and 48 (Fig. 7C and D) h of incubation. The positive controls acetoacetate [29] and galactose [30] also increased mitophagy events.

Considering that autophagy has pleiotropic effects in cancer [40], we investigated whether RCT-induced autophagy was related to its cytotoxicity in HepG2 cells. Therefore, we initially investigated whether an autophagy inhibitor was able to prevent its cytotoxic effect. Chloroquine, a lysosomotropic agent that prevents autophagosome-lysosome fusion in late-stage autophagy [41], was used to inhibit autophagic flux in RCT-treated HepG2 cells, and cell viability was measured after 48 h of incubation. Interestingly, chloroquine partly prevented RCT-induced cell death in HepG2 cells (Fig. 8A and B), indicating that RCT induces autophagy-mediated cell death.

Moreover, the role of autophagy in RCT-induced cell death was examined in *Atg5*$^{-/-}$ MEFs, which are MEFs with *Atg5* gene knockout, and parental wild-type MEFs [42], as well as in PentaKO HeLa cells, which are human cervical adenocarcinomas with five autophagy receptor knockouts (TAX1BP1, NDP52 [also known as CALCOCO2], NBR1, p62/SQSTM1, and OPTN), and parental wild-type HeLa cells [43].

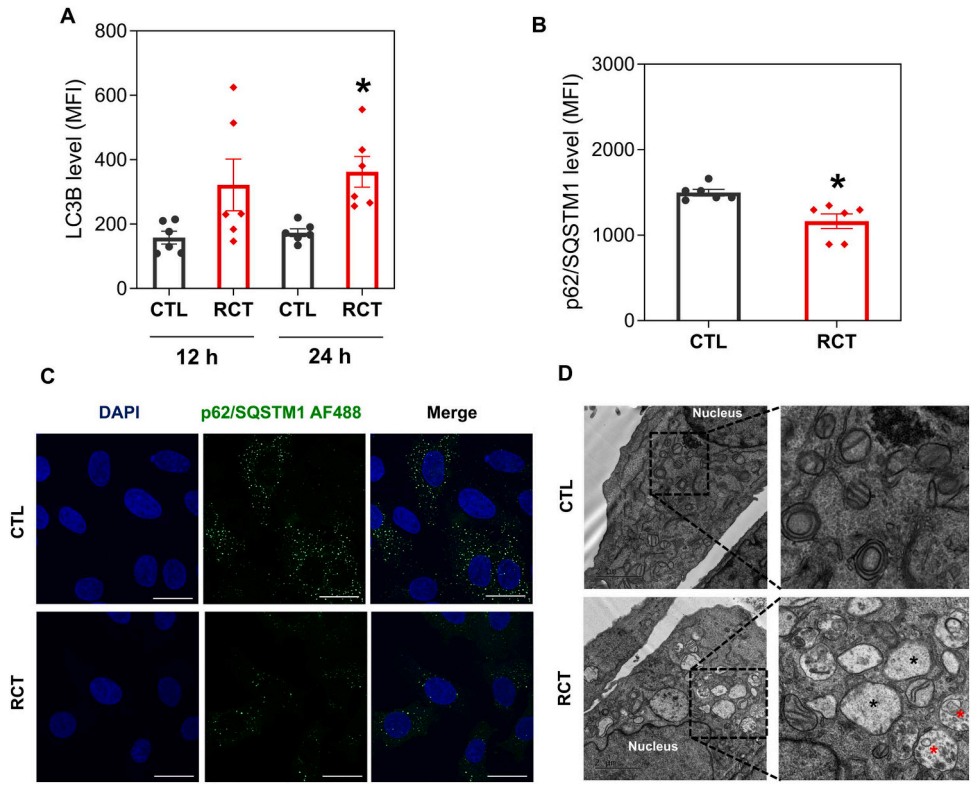

Fig. 6. Quantification of LC3B (A) and p62/SQSTM1 (B) expressions in HepG2 cells after 24 h of incubation with 4 μM RCT, as determined by flow cytometric analysis. The vehicle (0.2 % DMSO) was used as a control (CTL). The data are reported as the mean ± S.E.M. from three independent experiments, each performed in duplicate. * $P < 0.05$ compared to CTL by Student's *t* test. MFI: Mean fluorescence intensity. (C) Representative immunofluorescence images of p62/SQSTM1 in HepG2 cells after 24 h of incubation with 4 μM RCT. Scale bar = 25 μm. (D) Representative MET images of HepG2 cells after 12 h of incubation with 4 μM RCT. Black asterisks represent empty vacuoles, and red asterisks represent autophagic vacuoles. Scale bar = 2 μm.

Wild-type MEFs (Supplementary Figure 6) and wild-type HeLa cells (Supplementary Figure 7) were more sensitive to RCT-induced cytotoxicity than their mutant cell lines, *Atg5*$^{-/-}$ MEFs and PentaKO HeLa cells, respectively, corroborating that RCT induces autophagy-mediated cell death.

Moreover, wild-type HeLa cells treated with chloroquine, bafilomycin A1 (a lysosomotropic agent that prevents fusion between autophagosomes and lysosomes in the final stage of autophagy) or 3-MA (an early-stage autophagy inhibitor that blocks autophagosome formation by inhibiting PI3K) [41] became less sensitive to RCT-induced cytotoxicity (Supplementary Figure 8). All these data corroborate that cell death induced by RCT is, at least in part, mediated by autophagy.

4. Discussion

Herein, we demonstrated that RCT displays potent cytotoxicity to solid and haematological cancer cell lines, causes the elimination of hepatic CSCs from HepG2 cells, inhibits HepG2 cell motility, suppresses Akt/mTOR signalling and induces apoptotic and autophagic cell death in HepG2 cells. The ability of RCT to suppress hepatic CSCs, target Akt/mTOR signalling and cause autophagic cell death in HepG2 cells was reported for the first time in this study.

As mentioned above, RCT is a novel ruthenium complex containing a 1,3-thiazolidine-2-thione ligand that has been previously reported to have potent cytotoxic effects on cancer cells of different histological types [20–22]. Here, we report that this molecule can suppress hepatic CSCs. Previously, several different ruthenium complexes were reported to inhibit colorectal CSCs [44–47], glioma CSCs [48], breast CSCs [44], pancreatic CSCs [49], and hepatic CSCs [19].

CSCs exhibit cell motility and metastatic potential [34]. Interestingly, RCT inhibited HepG2 cell motility, indicating its antimetastatic potential. Previously, Ru(II)-based complexes containing 2-thiouracil derivatives were shown to inhibit HepG2 cell motility [19]. Polypyridyl Ru(II) complexes have also been reported to inhibit migration and invasion potential in melanoma and breast cancer cells [50], while Ru(II) carbonyl complexes reduce migration and invasion in HepG2 cells [51], and a ruthenium complex with 5-fluorouracil [46] and a ruthenium-xanthoxylin complex [47] reduce migration and invasion in colorectal cancer cells.

In addition, RCT has been reported to be a topoisomerase IB enzyme inhibitor [21] that causes ERK1/2-mediated apoptosis via a ROS- and p53-independent pathway in HepG2 cells [22]. In this work, the ability of RCT to suppress Akt/mTOR signalling was also demonstrated. Curiously, drugs targeting Akt/mTOR signalling have been reported to eradicate CSCs [9,10,12,19,46,47].

A Ru(II)-tetrazolate arene complex inhibited PI3K/Akt/ERK signalling in colorectal cancer cells, promoting greater sensitivity to regorafenib cytotoxicity [52], while a Ru(II)-xanthoxylin complex induced ERK1/2-mediated apoptosis in HepG2 cells via a p53-independent mechanism [14]. Bomfim et al. [16] reported that Ru(II) complexes with 6-methyl-2-thiouracil induce DNA double-strand breaks and trigger caspase-mediated apoptosis through the JNK/p38 pathway in leukaemia cells. The ruthenium complex with 5-fluorouracil inhibited Akt/mTOR signalling in colorectal cancer cells [46], while the Ru(II)-xanthoxylin complex suppressed the HSP90 chaperone in colorectal cancer cells [47].

In addition to apoptosis, RCT also induces autophagy, including mitophagy. The ability of RCT to induce apoptosis has been previously reported [22]; however, RCT-induced autophagy has never been explored. Although autophagy is a biological process of survival, it has also been characterized as a mechanism of cell death [40,53,54]. The Nomenclature Committee on Cell Death (NCCD) describes autophagy as

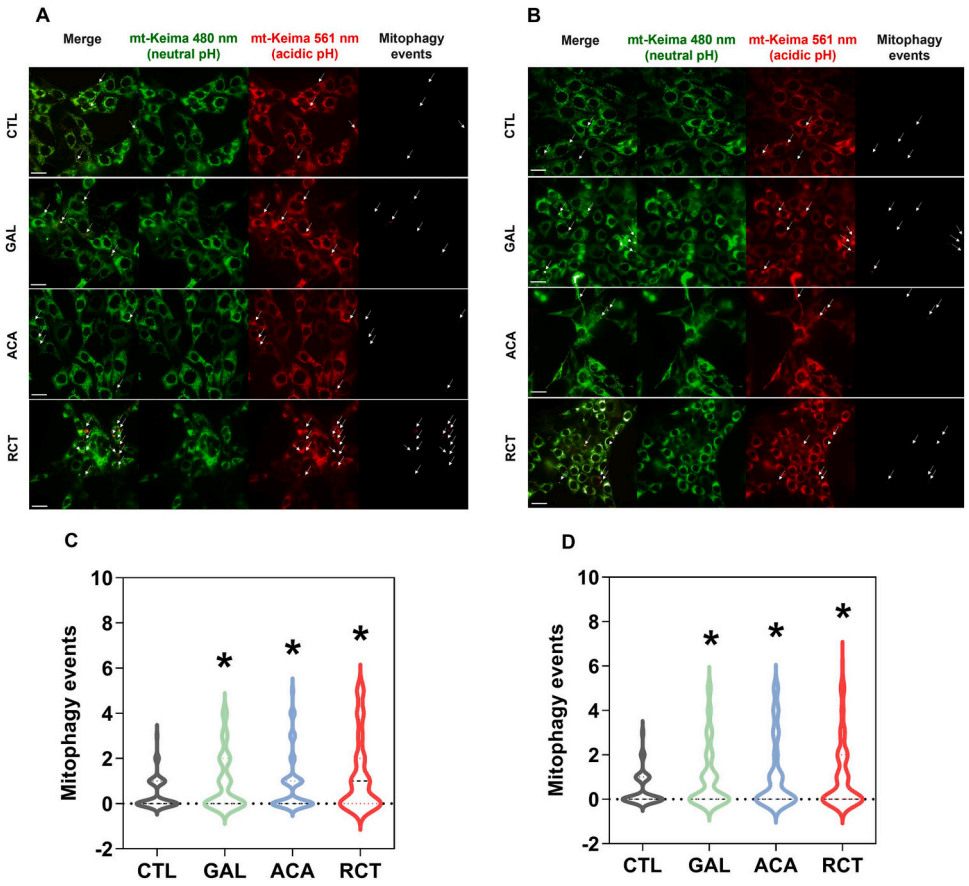

Fig. 7. Quantification of mitophagy in wild-type MEFs expressing mt-Keima after 24 (A and C) and 48 (B and D) h of incubation with 2 μM RCT. Culture medium containing glucose was used as a negative control (CTL). Galactose (GAL) and acetoacetate (ACA) media were used as positive controls. Scale bar = 20 μm. The data are displayed as cell popular violin plots from three independent repeats, each performed in duplicate. * $P < 0.05$ compared to CTL by one-way ANOVA followed by Dunnett's multiple comparisons test.

controlled cell death that is mechanically dependent on the autophagic machinery or its components to induce cell death. Therefore, autophagy-mediated cell death can be restored or prevented by pharmacological or genetic manipulation [40,54].

Herein, we demonstrated that RCT modulates the autophagy markers LC3B and p62/SQSTM1 in HepG2 cells and increases mitophagy events in a mt-Keima-transfected MEF model and that the cytotoxicity of RCT was partially prevented by autophagy inhibitors. In addition, mutant *Atg5*$^{-/-}$ MEFs and PentaKO HeLa cells are less sensitive to RCT cytotoxicity than their parental cell lines, indicating that RCT induces autophagy-mediated cell death. RCT reduced the levels of mTOR phosphorylated at Ser 2448, a negative modulator of autophagy [40], in HepG2 cells, suggesting that the ability of RCT to promote autophagy is due to its ability to regulate mTOR phosphorylation. Interestingly, the induction of autophagic cell death has been described as a target for the eradication of CSCs [40], indicating that RCT-induced autophagic cell death may contribute to its ability to eliminate CSCs.

Taken together, these data indicate that RCT is a novel potential anti-liver cancer drug that suppresses CSCs by targeting Akt/mTOR signalling and causing apoptotic and autophagic cell death.

Ethics approval and consent to participate

For human samples, the Research Ethics Committee of the Oswaldo Cruz Foundation (Salvador, Bahia, Brazil) (CAAE 16220713.2.0000.0040) approved the protocols. All subjects provided signed informed consent prior to the use of these clinical materials for research purposes. All methods were performed in accordance with the relevant guidelines and regulations.

CRediT authorship contribution statement

Alzir A. Batista: Writing – review & editing, Visualization, Supervision, Project administration, Funding acquisition, Data curation, Conceptualization. **Daniel P. Bezerra:** Writing – review & editing, Supervision, Project administration, Funding acquisition, Conceptualization. **Larissa M. Bomfim:** Writing – review & editing, Visualization, Validation, Investigation, Formal analysis. **Viktor I. Korolchuk:** Writing – review & editing, Visualization, Supervision, Project administration, Funding acquisition, Data curation, Conceptualization. **Sara P. Neves:** Writing – review & editing, Visualization, Validation, Investigation, Formal analysis, Conceptualization. **Sabrine G. Carvalho:** Writing – review & editing, Visualization, Validation, Investigation, Formal analysis. **Tetsushi Kataura:** Writing – review & editing, Visualization, Investigation, Formal analysis, Data curation. **Rosane B. Dias:** Writing – review & editing, Visualization, Methodology, Investigation, Formal analysis, Data curation. **Mateus L. Nogueira:** Writing – review & editing, Visualization, Validation, Investigation, Formal analysis. **Clarissa A. Gurgel Rocha:** Writing – review & editing, Visualization, Validation, Supervision, Project administration, Investigation, Funding acquisition, Conceptualization. **Ludmila de F. Valverde:** Writing – review & editing, Visualization, Methodology, Investigation, Formal analysis. **Monize M. da Silva:** Writing – review & editing, Visualization, Investigation, Formal analysis, Data curation. **Milena B. P. Soares:** Writing – review & editing, Visualization, Supervision, Project administration, Funding acquisition, Conceptualization.

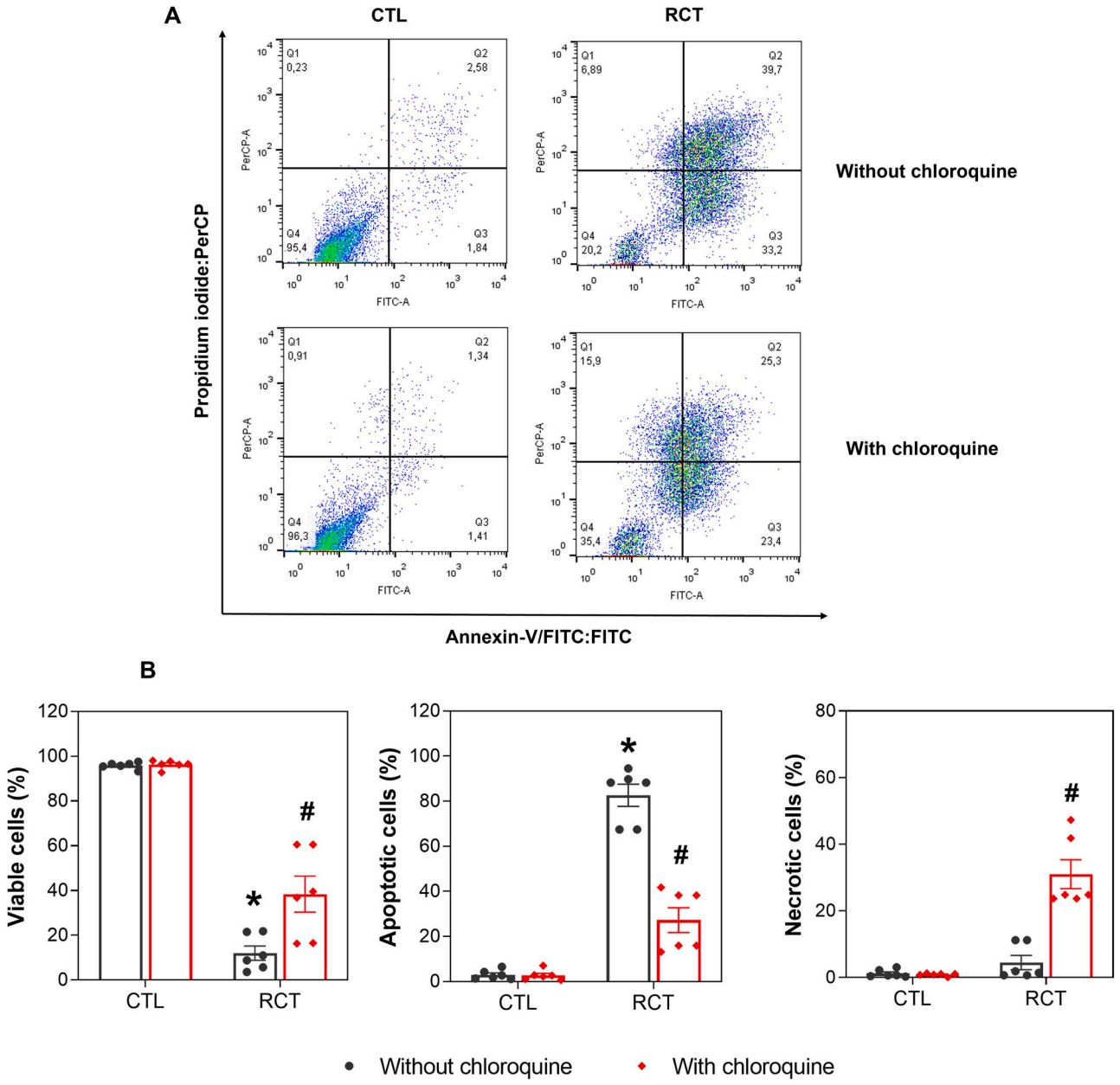

Fig. 8. Effect of chloroquine (an autophagy inhibitor) on RCT-induced cell death in HepG2 cells. (A) Representative flow cytometric dot plots. (B) Quantification of viable (annexin V-FITC/PI double-negative cells), apoptotic (annexin V-FITC-positive cells/PI-negative cells plus annexin V-FITC/PI double-positive cells), and necrotic (annexin V-FITC-negative cells/PI-positive cells) cells. The cells were pretreated with 40 μM chloroquine and then incubated with 4 μM RCT for 48 h. The vehicle (0.2 % DMSO) was used as a control (CTL). The data are reported as the mean ± S.E.M. from three independent experiments, each performed in duplicate. * $P < 0.05$ compared to CTL by Student's *t* test. # $P < 0.05$ compared to the respective treatment without inhibitor by Student's *t* test.

Declaration of Competing Interest

The authors declare the following financial interests/personal relationships which may be considered as potential competing interests: VIK is a scientific advisor for Longaevus Technologies. All other authors declare no competing interests.

Data availability

Data will be made available on request.

Acknowledgements

The authors would like to thank the FIOCRUZ-Bahia flow cytometry and microscopy cores for collecting flow cytometric data and acquiring confocal microscopy and MET data, respectively.

Financial support

This work received financial support and fellowships from the Brazilian agencies Coordenação de Aperfeiçoamento de Pessoal de Nível Superior (CAPES, code 001), Conselho Nacional de Desenvolvimento Científico e Tecnológico (CNPq, 307619/2021-4), Fundação à Pesquisa do Estado de São Paulo (FAPESP), Fundação à Pesquisa do Estado da Bahia (FAPESB), and Fundação Oswaldo Cruz (Programa INOVA-FIOCRUZ, VPPCB-007-FIO-18). TK received a fellowship from the Uehara Memorial Foundation and the International Medical Research Foundation (Japan).

Appendix A. Supporting information

Supplementary data associated with this article can be found in the online version at doi:10.1016/j.biopha.2024.117059.

References

[1] H. Rumgay, M. Arnold, J. Ferlay, O. Lesi, C.J. Cabasag, J. Vignat, M. Laversanne, K. A. McGlynn, I. Soerjomataram, Global burden of primary liver cancer in 2020 and predictions to 2040, J. Hepatol. 77 (6) (2022 Dec) 1598–1606, https://doi.org/10.1016/j.jhep.2022.08.021.

[2] J.M. Llovet, S. Ricci, V. Mazzaferro, P. Hilgard, E. Gane, J.F. Blanc, A.C. de Oliveira, A. Santoro, J.L. Raoul, A. Forner, M. Schwartz, C. Porta, S. Zeuzem, L. Bolondi, T.F. Greten, P.R. Galle, J.F. Seitz, I. Borbath, D. Häussinger, T. Giannaris, M. Shan, M. Moscovici, D. Voliotis, J. Bruix, SHARP Investigators Study Group, Sorafenib in advanced hepatocellular carcinoma, N. Engl. J. Med. 359 (4) (2008 Jul 24) 378–390, https://doi.org/10.1056/NEJMoa0708857.

[3] M. Kudo, R.S. Finn, S. Qin, K.H. Han, K. Ikeda, F. Piscaglia, A. Baron, J.W. Park, G. Han, J. Jassem, J.F. Blanc, A. Vogel, D. Komov, T.R.J. Evans, C. Lopez, C. Dutcus, M. Guo, K. Saito, S. Kraljevic, T. Tamai, M. Ren, A.L. Cheng, Lenvatinib versus sorafenib in first-line treatment of patients with unresectable hepatocellular carcinoma: a randomised phase 3 non-inferiority trial, Lancet 391 (10126) (2018 Mar 24) 1163–1173, https://doi.org/10.1016/S0140-6736(18)30207-1.

[4] A. Villanueva, Hepatocellular carcinoma, N. Engl. J. Med. 380 (15) (2019 Apr 11) 1450–1462, https://doi.org/10.1056/NEJMra1713263.

[5] J.M. Llovet, R.K. Kelley, A. Villanueva, A.G. Singal, E. Pikarsky, S. Roayaie, R. Lencioni, K. Koike, J. Zucman-Rossi, R.S. Finn, Hepatocellular carcinoma, Nat. Rev. Dis. Prim. 7 (1) (2021 Jan 21) 6, https://doi.org/10.1038/s41572-020-00240-3.

[6] J. Bruix, S. Qin, P. Merle, A. Granito, Y.H. Huang, G. Bodoky, M. Pracht, O. Yokosuka, O. Rosmorduc, V. Breder, R. Gerolami, G. Masi, P.J. Ross, T. Song, J. P. Bronowicki, I. Ollivier-Hourmand, M. Kudo, A.L. Cheng, J.M. Llovet, R.S. Finn, M.A. LeBerre, A. Baumhauer, G. Meinhardt, G. Han, RESORCE Investigators, Regorafenib for patients with hepatocellular carcinoma who progressed on sorafenib treatment (RESORCE): a randomised, double-blind, placebo-controlled, phase 3 trial, Lancet 389 (10064) (2017 Jan 7) 56–66, https://doi.org/10.1016/S0140-6736(16)32453-9.

[7] G.K. Abou-Alfa, T. Meyer, A.L. Cheng, A.B. El-Khoueiry, L. Rimassa, B.Y. Ryoo, I. Cicin, P. Merle, Y. Chen, J.W. Park, J.F. Blanc, L. Bolondi, H.J. Klümpen, S. L. Chan, V. Zagonel, T. Pressiani, M.H. Ryu, A.P. Venook, C. Hessel, A.E. Borgman-Hagey, G. Schwab, R.K. Kelley, Cabozantinib in patients with advanced and progressing hepatocellular carcinoma, N. Engl. J. Med. 379 (1) (2018 Jul 5) 54–63, https://doi.org/10.1056/NEJMoa1717002.

[8] A.X. Zhu, Y.K. Kang, C.J. Yen, R.S. Finn, P.R. Galle, J.M. Llovet, E. Assenat, G. Brandi, M. Pracht, H.Y. Lim, K.M. Rau, K. Motomura, I. Ohno, P. Merle, B. Daniele, D.B. Shin, G. Gerken, C. Borg, J.B. Hiriart, T. Okusaka, M. Morimoto, Y. Hsu, P.B. Abada, M. Kudo, REACH-2 study investigators, Ramucirumab after sorafenib in patients with advanced hepatocellular carcinoma and increased α-fetoprotein concentrations (REACH-2): a randomised, double-blind, placebo-controlled, phase 3 trial, Lancet Oncol. 20 (2) (2019 Feb) 282–296, https://doi.org/10.1016/S1470-2045(18)30937-9.

[9] L. Yang, P. Shi, G. Zhao, J. Xu, W. Peng, J. Zhang, G. Zhang, X. Wang, Z. Dong, F. Chen, H. Cui, Targeting cancer stem cell pathways for cancer therapy, Signal Transduct. Target Ther. 5 (1) (2020 Feb 7) 8, https://doi.org/10.1038/s41392-020-0110-5.

[10] V.R. Silva, L.S. Santos, R.B. Dias, C.A. Quadros, D.P. Bezerra, Emerging agents that target signalling pathways to eradicate colorectal cancer stem cells. Cancer Commun. 41 (12) (2021 Dec) 1275–1313, https://doi.org/10.1002/cac2.12235.

[11] T.K. Lee, X.Y. Guan, S. Ma, Cancer stem cells in hepatocellular carcinoma - from origin to clinical implications, Nat. Rev. Gastroenterol. Hepatol. 19 (1) (2022 Jan) 26–44, https://doi.org/10.1038/s41575-021-00508-3.

[12] A.C.B.D.C. Rodrigues, R.G.A. Costa, S.L.R. Silva, I.R.S.B. Dias, R.B. Dias, D. P. Bezerra, Cell signaling pathways as molecular targets to eliminate AML stem cells, Crit. Rev. Oncol. Hematol. 160 (2021 Apr) 103277, https://doi.org/10.1016/j.critrevonc.2021.103277.

[13] R.G.A. Costa, S.L.R. Silva, I.R.S.B. Dias, M.S. Oliveira, A.C.B.D.C. Rodrigues, R. B. Dias, D.P. Bezerra, Emerging drugs targeting cellular redox homeostasis to eliminate acute myeloid leukemia stem cells, Redox Biol. 62 (2023 Jun) 102692, https://doi.org/10.1016/j.redox.2023.102692.

[14] N.C. Carvalho, S.P. Neves, R.B. Dias, L.F. Valverde, C.B.S. Sales, C.A.G. Rocha, M.B. P. Soares, E.R. Dos Santos, R.M.M. Oliveira, R.M. Carlos, P.C.L. Nogueira, D. P. Bezerra, A novel ruthenium complex with xanthoxylin induces S-phase arrest and causes ERK1/2-mediated apoptosis in HepG2 cells through a p53-independent pathway, Cell Death Dis. 9 (2) (2018 Jan 23) 79, https://doi.org/10.1038/s41419-017-0104-6.

[15] V.R. Silva, R.S. Corrêa, L.S. Santos, M.B.P. Soares, A.A. Batista, D.P. Bezerra, A ruthenium-based 5-fluorouracil complex with enhanced cytotoxicity and apoptosis induction action in HCT116 cells, Sci. Rep. 8 (1) (2018 Jan 10) 288, https://doi.org/10.1038/s41598-017-18639-6.

[16] L.M. Bomfim, F.A. de Araujo, R.B. Dias, C.B.S. Sales, C.A.G. Rocha, R.S. Correa, M. B.P. Soares, A.A. Batista, D.P. Bezerra, Ruthenium(II) complexes with 6-methyl-2-thiouracil selectively reduce cell proliferation, cause DNA double-strand break and trigger caspase-mediated apoptosis through JNK/p38 pathways in human acute promyelocytic leukemia cells, Sci. Rep. 9 (1) (2019 Aug 7) 11483, https://doi.org/10.1038/s41598-019-47914-x.

[17] H. Tang, X. Guo, W. Yu, J. Gao, X. Zhu, Z. Huang, W. Ou, H. Zhang, L. Chen, J. Chen, Ruthenium(II) complexes as mitochondrial inhibitors of topoisomerase induced A549 cell apoptosis, J. Inorg. Biochem 246 (2023 Jun 15) 112295, https://doi.org/10.1016/j.jinorgbio.2023.112295.

[18] O.A. Lenis Rojas, S. Cordeiro, P.V. Baptista, A.R. Fernandes, Half-sandwich Ru(II) N-heterocyclic carbene complexes in anticancer drug design, J. Inorg. Biochem 245 (2023 Aug) 112255, https://doi.org/10.1016/j.jinorgbio.2023.112255.

[19] L.M. Bomfim, S.P. Neves, A.M.R.M. Coelho, M.L. Nogueira, R.B. Dias, L. F. Valverde, C.A.G. Rocha, M.B.P. Soares, A.A. Batista, R.S. Correa, D.P. Bezerra, Ru(II)-based complexes containing 2-thiouracil derivatives suppress liver cancer stem cells by targeting NF-κB and Akt/mTOR signaling, Cell Death Discov. 10 (1) (2024 Jun 3) 270, https://doi.org/10.1038/s41420-024-02036-w.

[20] R.S. Correa, M.M. da Silva, A.E. Graminha, C.S. Meira, J.A. Santos, D.R. Moreira, M.B. Soares, G. Von Poelhsitz, E.E. Castellano, C. Bloch Jr, M.R. Cominetti, A. A. Batista, Ruthenium(II) complexes of 1,3-thiazolidine-2-thione: cytotoxicity against tumor cells and anti-Trypanosoma cruzi activity enhanced upon combination with benznidazole, J. Inorg. Biochem 156 (2016 Mar) 153–163, https://doi.org/10.1016/j.jinorgbio.2015.12.024.

[21] M.M. Silva, M.S. de Camargo, R.S. Correa, S. Castelli, R.A. De Grandis, J. E. Takarada, E.A. Varanda, E.E. Castellano, V.M. Deflon, M.R. Cominetti, A. Desideri, A.A. Batista, Non-mutagenic Ru(II) complexes: cytotoxicity, topoisomerase IB inhibition, DNA and HSA binding, Dalton Trans. 48 (39) (2019 Oct 7) 14885–14897, https://doi.org/10.1039/c9dt01905g.

[22] S.P. Neves, N.C. de Carvalho, M.M. da Silva, A.C.B.C. Rodrigues, L.M. Bomfim, R. B. Dias, C.B.S. Sales, C.A.G. Rocha, M.B.P. Soares, A.A. Batista, D.P. Bezerra, Ruthenium complexes containing heterocyclic thioamidates trigger caspase-mediated apoptosis through MAPK signalling in human hepatocellular carcinoma cells. Front. Oncol. 9 (9) (2019 Jul) 562, https://doi.org/10.3389/fonc.2019.00562.

[23] ATCC Animal Cell Culture Guide. Get time-tested tips for culturing ATCC animal cells. 2024. ⟨https://www.atcc.org/resources/culture-guides/animal-cell-culture-guide⟩. Accessed in june 2024.

[24] S.A. Ahmed, R.M. Gogal Jr, J.E. Walsh, A new rapid and simple non-radioactive assay to monitor and determine the proliferation of lymphocytes: an alternative to [3H]thymidine incorporation assay, J. Immunol. Methods 170 (1994) 211–224, https://doi.org/10.1016/0022-1759(94)90396-4.

[25] I. Nicoletti, G. Migliorati, M.C. Pagliacci, F. Grignani, C. Riccardi, A rapid and simple method for measuring thymocyte apoptosis by propidium iodide staining and flow cytometry, J. Immunol. Methods 139 (2) (1991 Jun 3) 271–279, https://doi.org/10.1016/0022-1759(91)90198-o.

[26] R.R. Burk, A factor from a transformed cell line that affects cell migration, Proc. Natl. Acad. Sci. USA 70 (2) (1973 Feb) 369–372, https://doi.org/10.1073/pnas.70.2.369.

[27] J. Marshall, Transwell(®) invasion assays, Methods Mol. Biol. 769 (2011) 97–110, https://doi.org/10.1007/978-1-61779-207-6_8.

[28] K.J. Livak, T.D. Schmittgen, Analysis of relative gene expression data using real-time quantitative PCR and the 2(-Delta Delta C(T)) Method, Methods 25 (4) (2001 Dec) 402–408, https://doi.org/10.1006/meth.2001.1262.

[29] Y.P. Abudu, B.K. Shrestha, W. Zhang, A. Palara, H.B. Brenne, K.B. Larsen, D. L. Wolfson, G. Dumitriu, C.I. Øie, B.S. Ahluwalia, G. Levy, C. Behrends, S.A. Tooze, S. Mouilleron, T. Lamark, T. Johansen, SAMM50 acts with p62 in piecemeal basal- and OXPHOS-induced mitophagy of SAM and MICOS components, J. Cell Biol. 220 (8) (2021 Aug 2) e202009092, https://doi.org/10.1083/jcb.202009092.

[30] T. Kataura, L. Sedlackova, E.G. Otten, R. Kumari, D. Shapira, F. Scialo, R. Stefanatos, K.I. Ishikawa, G. Kelly, E. Seranova, C. Sun, D. Maetzel, N. Kenneth, S. Trushin, T. Zhang, E. Trushina, C.C. Bascom, R. Tasseff, R.J. Isfort, J.E. Oblong, S. Miwa, M. Lazarou, R. Jaenisch, M. Imoto, S. Saiki, M. Papamichos-Chronakis, R. Manjithaya, O.D.K. Maddocks, A. Sanz, S. Sarkar, V.I. Korolchuk, Autophagy promotes cell survival by maintaining NAD levels, Dev. Cell 57 (22) (2022 Nov 21) 2584–2598.e11, https://doi.org/10.1016/j.devcel.2022.10.008.

[31] V. Rajendran, M.V. Jain, Invitro tumorigenic assay: colony forming assay for cancer stem cells, Methods Mol. Biol. 1692 (2018) 89–95, https://doi.org/10.1007/978-1-4939-7401-6_8.

[32] K. Nio, T. Yamashita, S. Kaneko, The evolving concept of liver cancer stem cells, Mol. Cancer 16 (1) (2017 Jan 30) 4, https://doi.org/10.1186/s12943-016-0572-9.

[33] A.P. Deshmukh, P. den Hollander, N.A. Kuburich, S. Vasaikar, R. Joseph, S. A. Mani, Enrichment of cancer stem cells in a tumorsphere assay, Methods Mol. Biol. 2429 (2022) 501–507, https://doi.org/10.1007/978-1-0716-1979-7_34.

[34] T. Celià-Terrassa, M.K. Jolly, Cancer stem cells and epithelial-to-mesenchymal transition in cancer metastasis, Cold Spring Harb. Perspect. Med. 10 (7) (2020 Jul 1) a036905, https://doi.org/10.1101/cshperspect.a036905.

[35] S. Jayaraman, X. Wu, K.R. Kalari, X. Tang, M.J. Kuffel, E.S. Bruinsma, S. Jalali, K. L. Peterson, C. Correia, R.A. Kudgus, S.H. Kaufmann, S. Renuse, J.N. Ingle, J. M. Reid, M.M. Ames, A.P. Fields, M.J. Schellenberg, J.R. Hawse, A. Pandey, M. P. Goetz, Endoxifen downregulates AKT phosphorylation through protein kinase C beta 1 inhibition in ERα+ breast cancer, NPJ Breast Cancer 9 (1) (2023 Dec 19) 101, https://doi.org/10.1038/s41523-023-00606-2.

[36] A. Oeckinghaus, M.S. Hayden, S. Ghosh, Crosstalk in NF-κB signaling pathways, Nat. Immunol. 12 (8) (2011 Jul 19) 695–708, https://doi.org/10.1038/ni.2065.

[37] X. Yu, J.F. Robinson, E. Gribble, S.W. Hong, J.S. Sidhu, E.M. Faustman, Gene expression profiling analysis reveals arsenic-induced cell cycle arrest and apoptosis in p53-proficient and p53-deficient cells through differential gene pathways, Toxicol. Appl. Pharm. 233 (3) (2008 Dec 15) 389–403, https://doi.org/10.1016/j.taap.2008.09.016.

[38] X. Yu, J.F. Robinson, J.S. Sidhu, S. Hong, E.M. Faustman, A system-based comparison of gene expression reveals alterations in oxidative stress, disruption of ubiquitin-proteasome system and altered cell cycle regulation after exposure to cadmium and methylmercury in mouse embryonic fibroblast, Toxicol. Sci. 114 (2) (2010 Apr) 356–377, https://doi.org/10.1093/toxsci/kfq003.
[39] N. Sun, D. Malide, J. Liu, I.I. Rovira, C.A. Combs, T. Finkel, A fluorescence-based imaging method to measure in vitro and in vivo mitophagy using mt-Keima, Nat. Protoc. 12 (8) (2017 Aug) 1576–1587, https://doi.org/10.1038/nprot.2017.060.
[40] V.R. Silva, S.P. Neves, L.S. Santos, R.B. Dias, D.P. Bezerra, Challenges and therapeutic opportunities of autophagy in cancer therapy, Cancers 12 (11) (2020 Nov 20) 3461, https://doi.org/10.3390/cancers12113461.
[41] D.J. Klionsky, et al., Guidelines for the use and interpretation of assays for monitoring autophagy (4th edition)1, Autophagy 17 (1) (2021 Jan) 1–382, https://doi.org/10.1080/15548627.2020.1797280.
[42] A. Kuma, M. Hatano, M. Matsui, A. Yamamoto, H. Nakaya, T. Yoshimori, Y. Ohsumi, T. Tokuhisa, N. Mizushima, The role of autophagy during the early neonatal starvation period, Nature 432 (7020) (2004 Dec 23) 1032–1036, https://doi.org/10.1038/nature03029.
[43] M. Lazarou, D.A. Sliter, L.A. Kane, S.A. Sarraf, C. Wang, J.L. Burman, D.P. Sideris, A.I. Fogel, R.J. Youle, The ubiquitin kinase PINK1 recruits autophagy receptors to induce mitophagy, Nature 524 (7565) (2015 Aug 20) 309–314, https://doi.org/10.1038/nature14893.
[44] B. Purushothaman, P. Arumugam, H. Ju, G. Kulsi, A.A.S. Samson, J.M. Song, Novel ruthenium(II) triazine complex [Ru(bdpta)(tpy)]2+ co-targeting drug resistant GRP78 and subcellular organelles in cancer stem cells, Eur. J. Med Chem. 156 (2018 Aug 5) 747–759, https://doi.org/10.1016/j.ejmech.2018.07.048.
[45] S. Acharya, S. Ghosh, M. Maji, A.R.U. Parambil, S. Singh, A. Mukherjee, Inhibition of 3D colon cancer stem cell spheroids by cytotoxic RuII-p-cymene complexes of mesalazine derivatives, Chem. Commun. 56 (40) (2020 May 19) 5421–5424, https://doi.org/10.1039/d0cc00472c.
[46] V.R. Silva, L.S. Santos, M.V.L. de Castro, R.B. Dias, L.F. Valverde, C.A.G. Rocha, M. B.P. Soares, C.A. Quadros, R.S. Correa, A.A. Batista, D.P. Bezerra, A novel ruthenium complex with 5-fluorouracil suppresses colorectal cancer stem cells by inhibiting Akt/mTOR signaling, Cell Death Discov. 9 (1) (2023 Dec 16) 460, https://doi.org/10.1038/s41420-023-01759-6.
[47] L.S. Santos, V.R. Silva, M.V.L. de Castro, R.B. Dias, L.F. Valverde, C.A.G. Rocha, M. B.P. Soares, C.A. Quadros, E.R. Dos Santos, R.M.M. Oliveira, R.M. Carlos, P.C. L. Nogueira, D.P. Bezerra, New ruthenium-xanthoxylin complex eliminates colorectal cancer stem cells by targeting the heat shock protein 90 chaperone, Cell Death Dis. 14 (12) (2023 Dec 15) 832, https://doi.org/10.1038/s41419-023-06330-w.
[48] P. Elumalai, N. Kaushik, D.H. Kim, H. Kim, S.J. Lee, E.H. Choi, K.W. Chi, N. K. Kaushik, Flexible ligated ruthenium(II) self-assemblies sensitizes glioma tumor initiating cells in vitro, Oncotarget 8 (36) (2017 Jul 5) 60188–60200, https://doi.org/10.18632/oncotarget.19028.
[49] S. Alcalá, L. Villarino, L. Ruiz-Cañas, J.R. Couceiro, M. Martínez-Calvo, A. Palencia-Campos, D. Navarro, P. Cabezas-Sainz, I. Rodriguez-Arabaolaza, A. Cordero-Barreal, L. Trilla-Fuertes, J.A. Rubiolo, S. Batres-Ramos, M. Vallespinos, C. González-Páramos, J. Rodríguez, A. Gámez-Pozo, J.Á.F. Vara, S.F. Fernández, A. B. Berlinches, N. Moreno-Mata, A.M.T. Redondo, A. Carrato, P.C. Hermann, L. Sánchez, S. Torrente, M.Á. Fernández-Moreno, J.L. Mascareñas, B. Sainz Jr, Targeting cancer stem cell OXPHOS with tailored ruthenium complexes as a new anti-cancer strategy, J. Exp. Clin. Cancer Res. 43 (1) (2024 Jan 27) 33, https://doi.org/10.1186/s13046-023-02931-7.
[50] I. Gurgul, E. Janczy-Cempa, O. Mazuryk, M. Lekka, M. Łomzik, F. Suzenet, P. C. Gros, M. Brindell, Inhibition of metastasis by polypyridyl Ru(II) complexes through modification of cancer cell adhesion - in vitro functional and molecular studies, J. Med. Chem. 65 (15) (2022 Aug 11) 10459–10470, https://doi.org/10.1021/acs.jmedchem.2c00580.
[51] Y. Lu, T. Shen, H. Yang, W. Gu, Ruthenium complexes induce HepG2 human hepatocellular carcinoma cell apoptosis and inhibit cell migration and invasion through regulation of the Nrf2 pathway, Int. J. Mol. Sci. 17 (5) (2016 May 19) 775, https://doi.org/10.3390/ijms17050775.
[52] D. Sharma, F. Rasool, M. Bharti, K.M. Vyas, S.K.J. Magani, Regorafenib and ruthenium complex combination inhibit cancer cell growth by targeting PI3K/AKT/ERK signalling in colorectal cancer cells, Int. J. Mol. Sci. 24 (1) (2022 Dec 30) 686, https://doi.org/10.3390/ijms24010686.
[53] P.M.P. Ferreira, R.W.R. Sousa, J.R.O. Ferreira, G.C.G. Militão, D.P. Bezerra, Chloroquine and hydroxychloroquine in antitumor therapies based on autophagy-related mechanisms, Pharm. Res. 168 (2021 Jun) 105582, https://doi.org/10.1016/j.phrs.2021.105582.
[54] L. Galluzzi, et al., Molecular mechanisms of cell death: recommendations of the Nomenclature Committee on Cell Death, Cell Death Differ. 25 (3) (2018) 486–541, https://doi.org/10.1038/s41418-017-0012-4.